AIAA 82-4001

Aerodynamic Forces on Finite Wings in Oblique Gusts

M. H. Patel*
University College London, London, England

Experimental data comprising unsteady lift, pitching moment and rolling moments are presented for a set of three finite wing planforms immersed in two-dimensional oscillating gusts which are incident at oblique angles of up to 20 deg from the wing centerline. The effects of the resultant asymmetric lift distribution on the two wing halves are identified in the results with particular reference to the amplitudes and phases of rolling moment that are generated.

Nomenclature

$\mathcal{R}$ = aspect ratio = b^2/S
b = wing span (tip-to-tip)
C_L = lift coefficient = $L/\frac{1}{2}\rho U^2 S$
C_{PM} = pitching moment coefficient about a line through the root quarter chord point = $M_P/\frac{1}{2}\rho U^2 Sc$
C_{RM} = rolling moment coefficient about the wing centerline = $M_R/\frac{1}{2}\rho U^2 Sc$
c = streamwise wing chord
L = lift force
M_P = pitching moment about a line through the root quarter chord point
M_R = rolling moment about wing centerline
S = wing area in plan
t = time coordinate
U = mean freestream velocity
w = instantaneous vertical (downwash) velocity component of gust
$\bar{w}$ = instantaneous angle of incident gust = w/U
w_g = amplitude of vertical (downwash) velocity component in oscillatory flow
$\bar{w}_g$ = amplitude of incident gust angle in oscillatory flow = w_g/U
x, y, z = Cartesian frame of reference, fixed in the wing, as shown in Fig. 2
ΔC_L = amplitude of lift coefficient = $\Delta L/\frac{1}{2}\rho U^2 S$
ΔC_{PM} = amplitude of pitching moment coefficient about a line through the root quarter chord point = $\Delta M_P/\frac{1}{2}\rho U^2 Sc$
ΔC_{RM} = amplitude of rolling moment coefficient about wing centerline = $\Delta M_R/\frac{1}{2}\rho U^2 Sc$
ΔL = amplitude of lift
ΔM_P = amplitude of pitching moment about a line through the root quarter chord point
ΔM_R = amplitude of roll moment about the wing centerline
θ = wing skew angle (Fig. 2)
ν = frequency parameter = $\omega c/U$
ν' = "effective" frequency parameter = $\omega c/0.61\,U$
ρ = air density
ω = radian frequency

I. Introduction

In recent years, a quantitative knowledge of the aerodynamic forces on aircraft flying in atmospheric turbulence has been a continuing requirement. The fluctuating loads induced by atmospheric turbulence have a direct impact on the design of active control systems and in the development of aircraft structures that are more resistant to gust load induced fatigue failures. The latter need has been highlighted by current problems associated with the high-speed, low-altitude flight of military aircraft.

The development of analytical and numerical methods for predicting unsteady loads on aircraft wings in harmonic gusts has progressed significantly in the last decade. A wide range of reliable computations are now available to predict wing loads in oscillatory inviscid flow. References 1 and 2 present a useful overview of these methods. A number of theories[3,4] and complementary experimental results for finite wings in gusts have also been produced,[5-7] but no systematic comparisons between theory and experiment are available as yet. The aerodynamic problem of the two-dimensional airfoil in gusts has also been experimentally investigated.[8-11] In contrast to these studies, the forces and pressures on oscillating lifting surfaces in steady flow have been extensively researched, both theoretically and experimentally; again, Refs. 1 and 2 give further details.

An understanding of the intensity and nature of atmospheric turbulence commonly encountered by aircraft is crucial to the proper application of the above theories and supporting experiments. Reference 12 presents a collection of papers addressing this subject. The authors point out that the occurrence of turbulence is more likely to be intermittent with packets of high intensity turbulence (like discrete gusts) separated by longer quiescent periods rather than a continuous series of lower intensity disturbances. This raises the question of how an aerodynamic load calculation based on harmonic gusts can be applied to the incident discrete gust case. The results of experiments presented in Ref. 7 indicate that linear superposition of a series of harmonic gusts and their consequent load time histories is acceptable for attached

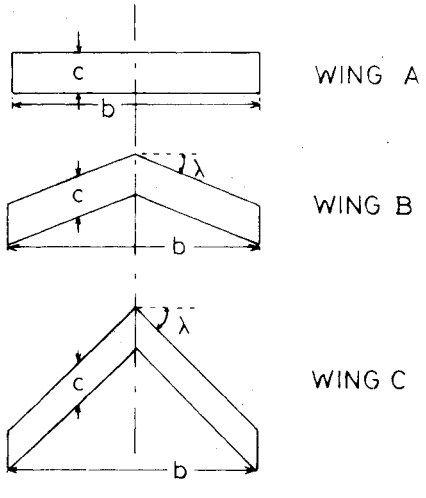

Fig. 1 Wing planforms.

Received Dec. 1, 1980; revision received June 9, 1981.

*Lecturer, Department of Mechanical Engineering. Member AIAA.

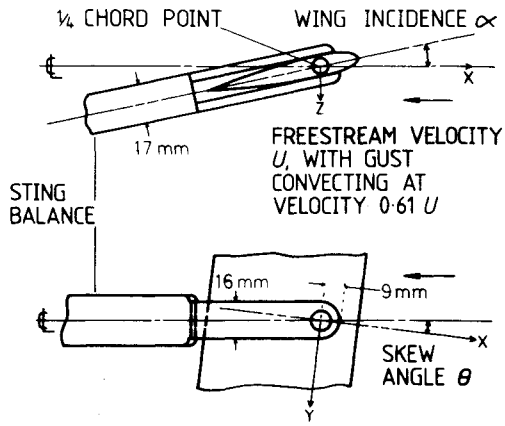

Fig. 2 Side and plan views of sting balance and wing model.

flow around finite wings. Reference 12 further emphasizes that the spectral distribution of measured atmospheric turbulence is such that significant spanwise incident gust variations are common. A highly simplified form of such a variation is an oblique gust approaching a wing, as indicated by Fig. 2. Conversely, the oblique gust can be regarded as occurring when an aircraft sideslips or yaws relative to an approaching gust front. In either case, the effective sweep angles of the two wing halves to the incident airflow become dissimilar, giving rise to induced unsteady roll moments. As a contribution to an understanding of the effects of oblique gusts, a series of measurements are presented for harmonic oblique gusts approaching three finite wings; all untapered and of aspect ratio 6 but with sweep angles of 0, 22.5, and 45 deg. It is hoped that these data will assist in the verification of theories attempting to model the physical reality.

II. Gust Tunnel Facility

A novel form of gust generation facility is used for these tests. Only the salient details of the facility are reproduced here. References 5 and 13 include extensive additional information.

The gust facility is based around a conventional wind tunnel with a working section which is 0.76 m high, 0.99 m across, and 2.6 m long. The gust generation device is sited at the upstream end of the working section. Its operation is based on perturbing shear layers above and below the semiopen working section (open top and bottom, rigid sidewalls) into rolling up and forming discrete vortices which convect downstream in the mixing region and induce an oscillatory travelling wave type of vertical gust in an irrotational flowfield within the working section.

The oscillatory vertical velocity component on the horizontal center plane of the working section can be written as

$$\bar{w}(x,t) = \bar{w}_g \exp[i\omega(t + x/0.61U)] \qquad (1)$$

where x is a coordinate pointing upstream, U is the mean freestream velocity, $\bar{w}$ is the nondimensionalized instantaneous vertical velocity component ($=w/U$), $\bar{w}_g$ is the nondimensionalized amplitude of vertical velocity oscillations, ω is the radian frequency, and $0.61\ U$ is the downstream convection velocity of the travelling wave. The gust convection velocity takes this particular value because the vortices which induce the gust are embedded in the mixing region of the semiopen jet working section (see Ref. 13 for further details).

The gust amplitude, $\bar{w}_g$, at the measuring station is an easily calibrated function of the shear layer perturbation frequency and amplitude. A usable frequency range, in terms of frequency parameter per unit chord (ω/U), of from 0.40 to 5.70 is available with gust amplitudes of $\bar{w}_g = 0.0314$ or 1.8 deg in gust incidence angle. The corresponding frequency values are between 2 and 12 Hz with the gust variations being closely sinusoidal in space and time (see Ref. 13).

Table 1 Planform dimensions

Wing	Span b, m	Streamwise chord c, m	Sweep angle λ, deg
A	0.60	0.10	0
B	0.60	0.10	22.5
C	0.60	0.10	45.0

The spatial distribution of gust amplitude in the vicinity of the model mounting position is such that the vertical velocity oscillations are two dimensional and substantially constant in the streamwise direction. The vertical variation of gust amplitude above and below the horizontal center plane of the working section exhibits a "hyperbolic cosine" type of variation with a nearly contant centerline gust amplitude which increases slowly with distance above and below the horizontal center plane. The hyperbolic cosine variation is due to the alternate rolled up vortices in the upper and lower mixing regions which induce the irrotational gust flow. However, this gust amplitude variation with vertical distance is not a limitation because of the thin wing models used in these experiments.

III. Test Models and Measurement Technique

The three planforms tested are shown in Fig. 1 with the dimensions given in Table 1. They were all untapered and of aspect ratio ($\mathcal{R}$) 6, with sweep angles of 0, 22.5, and 45 deg named as wings A, B, and C, respectively. The planforms were constructed using symmetrical 10% thick NACA 0010 airfoil sections with wing spans of 0.60 m, which was 60% of the working section width. The wings had straight leading and trailing edges with streamwise tips which were shaped such that the upper and lower wing surfaces were joined around each tip by a half body of revolution generated by the airfoil surface about the tip chord line. The wing streamwise chords were a constant 0.10 m for all three wings. Roughness strips were used to provoke transition just aft of the leading edges at 7% chord. These strips were 10 mm wide and were made up of silicon carbide abrasive paper with a grain height of 0.4 mm.

Figure 2 shows the reference axis system used for presenting the results. The origin is taken to be at the root quarter chord points of the wing planforms. For nonzero values of the skew angle θ, the coordinate axes rotate with the wings. Positive wing incidence is assumed to be nose-down to ensure consistency of "positive" lift with either wing incidence or downward gust velocity.

As shown in Fig. 2, the incident oblique gust was arranged by presenting the wings to the gust at varying angles of skew (in yaw) relative to the incident gust front.

Aerodynamic forces on the wings were measured by a cantilever-type lift, pitching moment, and rolling moment sensing sting balance. The balance had to be designed for very low strain levels and had to be of minimum length in order to maximize the natural frequencies in bending and torsional vibrations. Semiconductor strain gages with high gage factors (~ 180) and internal temperature compensation were used to maintain signal levels. Figure 2 presents details of the sting-wing mounting arrangement which allows the test planforms to be rotated at attitudes of skew of up to 20 deg relative to the incident gust field. A trunion enclosed within the wing root is clamped between forks which protrude from the sting onto the upper and lower surfaces at the wing root. The presence of the forks produces a small center body at the wing root which detracts from the preferred wing only configuration.

The effects on the measurements of oscillatory deflection of the sting-wing system under the imposed oscillating aerodynamic forces had to be calculated. The magnitude of the required correction to account for this were shown to be small owing to the combination of high sting stiffness and the

Table 2 Results of steady flow measurements

Wing planform	Force or moment slope	Experiment Skew angle, θ deg 0 deg	10 deg	20 deg	Inviscid theory (Ref. 14) 0 deg
A	$\partial C_L/\partial\alpha$	3.90	3.87	3.80	4.03
	$\partial C_{PM}/\partial\alpha$	0.0	0.0	0.0	0
	$\partial C_{RM}/\partial\alpha$	0.0	−0.23	−0.29	0
B	$\partial C_L/\partial\alpha$	3.73	3.83	3.84	4.02
	$\partial C_{PM}/\partial\alpha$	2.15	2.18	1.75	2.25
	$\partial C_{RM}/\partial\alpha$	−0.15	−0.63	−1.22	0
C	$\partial C_L/\partial\alpha$	2.91	2.87	2.71	3.35
	$\partial C_{PM}/\partial\alpha$	3.93	4.20	3.88	4.79
	$\partial C_{RM}/\partial\alpha$	−0.22	−1.05	−1.68	0

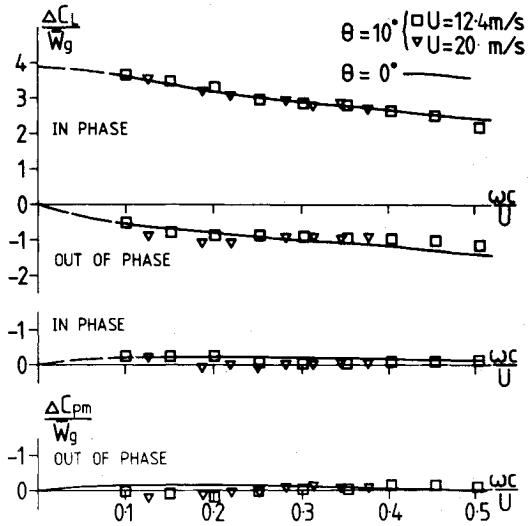

Fig. 3 Wing A, oscillating lift and pitching moment, $\alpha=0$ deg, $\theta=10$ deg.

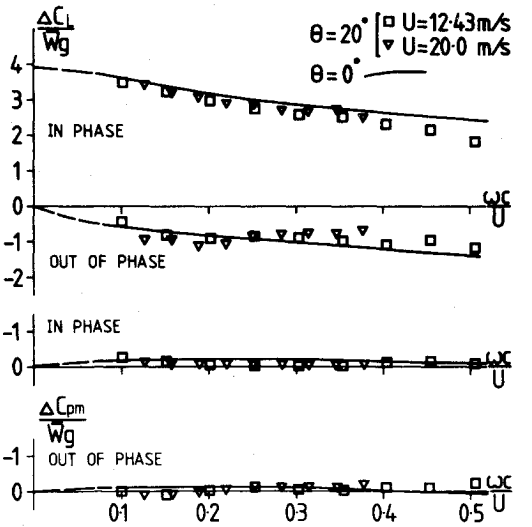

Fig. 4 Wing A, oscillating lift and pitching moment, $\alpha=0$ deg, $\theta=20$ deg.

small aerodynamic loads involved. The natural frequencies of the sting-wing system in bending and torsion were found to be 60 and 38 Hz, respectively. A measured dynamic calibration of each sting-wing combination required the amplitude of the oscillatory lift and roll moments to be corrected by up to 2% and 5%, respectively, at the highest test frequency (~12 Hz). The low damping present in the system produced negligible phase errors.

The measurements were made using an automated data sampling and processing system. The oscillatory force signals were sampled at selected time instants over successive oscillation cycles. A reference signal, from an upstream gust angle measuring yawmeter was used to supply the information needed to select the sampling time instants. The resulting data can be regarded as a set of "phase averages" defining the measured signal relative to a reference signal. A phase average is defined as the average value over successive cycles of the signal when sampled at a particular phase of the reference wave cycle. A numerical harmonic analysis of these data was employed to extract amplitude and phase information at the forcing frequency. After the application of calibration and correction factors, the final results are presented as in-phase and out-of-phase components of $\Delta C_L/\bar{w}_g$, $\Delta C_{PM}/\bar{w}_g$, and $\Delta C_{RM}/\bar{w}_g$ against frequency parameter $\nu=\omega c/U$ for each frequency of the input gust, where $\bar{w}_g$ is the amplitude of gust oscillation incident to the wing. The phase angles embedded in the data are relative to the undisturbed freestream flow at the wing root quarter chord points in the absence of the wings. A yawmeter positioned at this point was used to measure the freestream oscillatory gust relative to conditions at an upstream yawmeter. Force measurements were then made for each wing again relative to the upstream yawmeter output. A measure of the experimental uncertainty in the data can be put approximately as ±3% in amplitude and ±2 deg for phase angles. Reference 13 gives further details of the sampling and data processing apparatus.

IV. Experimental Results

The series of tests reported here were carried out in three parts.

Initially, experiments were conducted in oscillatory flow with the wings positioned symmetrically in the gust field (with $\theta=0$ deg) to verify that the data being collected conformed to previously acquired results (as in Ref. 5). This was followed by measurements in steady flow for all three wings at skew angles of $\theta=0$, 10, and 20 deg. The trends in measured lift, pitching moment, and rolling moments are presented in Table 2 in terms of the lift and moment curve slopes together with theoretical results for $\theta=0$ deg derived from Ref. 14. The values of rolling moment curve slope arose owing to the differential sweep of the two wing halves in the flow. This effect is small for rectangular wing A but is quite marked for wing C with a sweep angle of 45 deg. It is believed that the aerodynamic effects of the sting mount at the wing roots does lead to slightly lower values for lift curve slopes than those that would be obtained for the wing only configuration with no center body. This argument is supported by a comparison of theory and experiment for skew angle, $\theta=0$ deg. The experimental data also demonstrate the effects of sweep angle on the pitching and rolling moment derivatives. In particular for wings B and C, as the skew angle is increased, the difference in sweep angle of the two wing halves increases

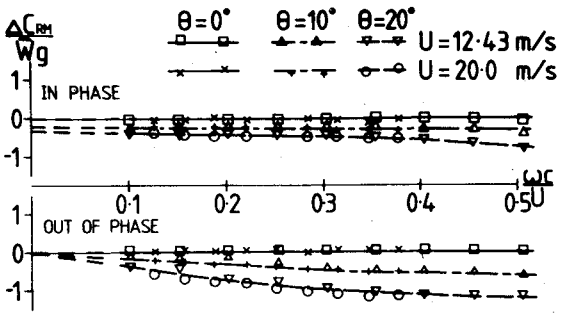

Fig. 5 Wing A, oscillating rolling moment, $\alpha = 0$ deg.

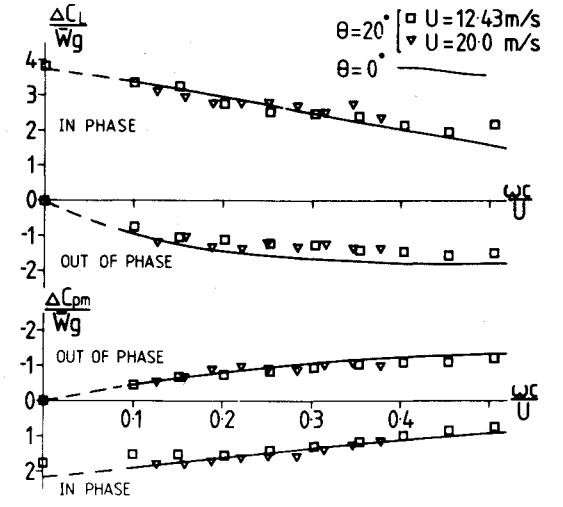

Fig. 6 Wing B, oscillating lift and pitching moment, $\alpha = 0$ deg, $\theta = 20$ deg.

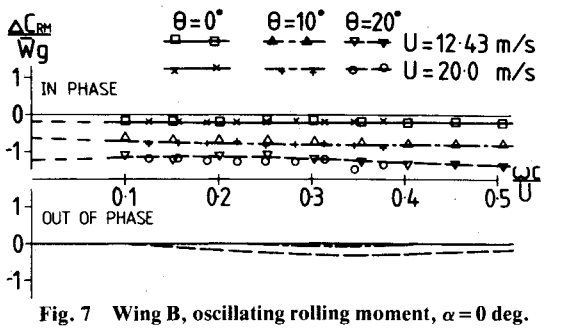

Fig. 7 Wing B, oscillating rolling moment, $\alpha = 0$ deg.

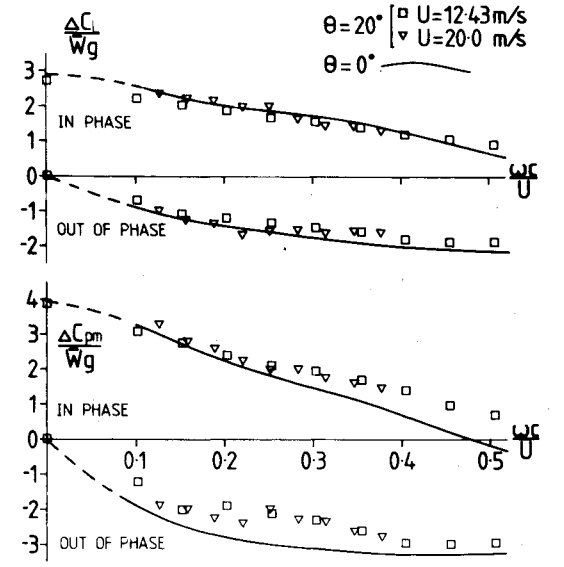

Fig. 8 Wing C, oscillating lift and pitching moment, $\alpha = 0$ deg, $\theta = 20$ deg.

together with changes in the moment arms for the lift forces on the wing halves. These two features lead to some apparently anomalous behavior in the data with $\partial C_L/\partial\alpha$ increasing with θ for wing B and $\partial C_{PM}/\partial\alpha$ having a maximum at $\theta = 10$ deg on wing C.

In the oscillatory flow tests for wing A, the lift and pitching moment distributions with frequency parameter at a skew angle of $\theta = 10$ deg were virtually identical to the symmetric response ($\theta = 0$ deg). Figure 3 indicates the level of agreement obtained. Figure 4 displays the same comparison for a skew angle of $\theta = 20$ deg, showing that these results do begin to differ markedly from the symmetric values. Significant effects of skew angle are evident in the rolling moment distributions presented in Figs. 5 and 11. Although the data are plotted as in-phase and out-of-phase components, it is to be noted that the rolling moment amplitude increases almost linearly with frequency parameter. The phase angle variation remains constant at around 110 deg lag for both skew angles of $\theta = 10$ and 20 deg. Both these amplitude and phase characteristics are consistent with the manner in which the rolling moment develops on the rectangular planform in an oscillatory oblique gust. The phase lag of 110 deg arises because, for a rectangular wing at an angle of skew, the gust induced oscillating rolling moment lags the oscillating lift on the wing halves by 90 deg and this lift force further lags the gust incidence angle by approximately 20 deg.

The oscillatory flow results for wing B are similar to those of wing A for lift and pitching moments. Figure 6 displays data for skew angles of $\theta = 0$ and 20 deg. The rolling moment variation is plotted in Fig. 7 for $\theta = 0$, 10, and 20 deg. A nonzero in-phase rolling moment at $\theta = 0$ deg indicates some asymmetry in the two wing halves. However, for $\theta = 10$ and 20 deg, the rolling moment changes mirror the differential lifts of the two wing halves owing to their sweep angles to the flow. These variations of wing B, unlike those of wing A, are not as clear-cut because the sweep of the two wing halves is no longer antisymmetric. However, the wing B rolling moments also exhibit a constant phase lag with frequency parameter of around 180 deg.

For wing C, Fig. 8 shows the lift and pitching moment variation against frequency parameter at skew angles of $\theta = 0$ and 20 deg. The results for $\theta = 10$ deg are virtually identical to the symmetric case ($\theta = 0$ deg). The rolling moment distributions for $\theta = 0$, 10, and 20 deg are shown in Fig. 9. Once again, small nonzero values are observed at $\theta = 0$ deg. However, the changes in rolling moment distribution with θ indicate a significant contribution of skew angle. As shown in Fig. 9, the amplitude remains virtually constant with frequency parameter for each skew angle, but unlike the result for wings A and B, the phase of rolling moment increases with frequency parameter. This would be expected from the much larger downstream extent of wing C which is being influenced by the streamwise incidence variation in the traveling gust field. The larger rolling moment amplitudes observed for wing C are a consequence of the highly asymmetric lift distribution that exists on the two wing halves.

The complete set of experimental data in oscillatory flow as described above were repeated with the wings set at an incidence of 3 deg. The results obtained were identical within experimental error bounds to the 0 deg incidence cases presented in Figs. 3-9.

Figures 10 and 11 display additional comparative plots of the experimental data. The effect of wing sweep on the measured lift amplitude variations against frequency parameter is illustrated by Fig. 10. The oscillatory lift is presented here as amplitude and phase in contrast to the in-phase and out-of-phase components plotted elsewhere. A similar comparative plot of the roll moments is shown in Fig.

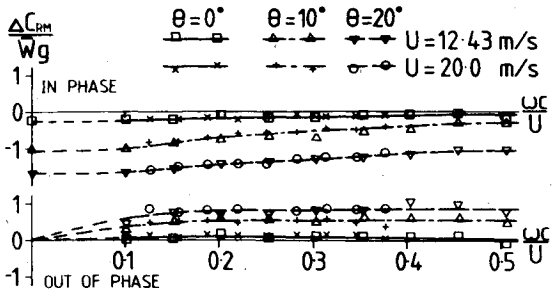

Fig. 9 Wing C, oscillating rolling moment, $\alpha = 0$ deg.

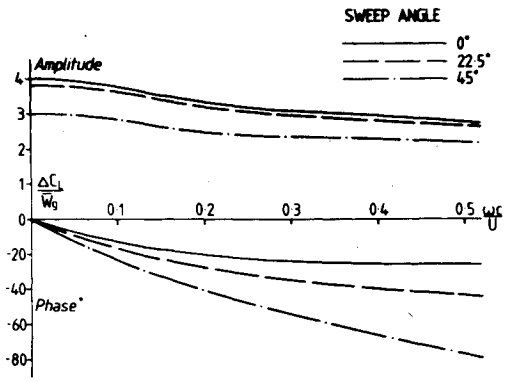

Fig. 10 Variation of oscillating lift with sweep angle.

11 for all three wings at the highest skew angle ($\theta = 20$ deg) used. In plotting the data by amplitude, other aspects of the rolling moment trends are revealed, particularly the variation of induced roll amplitude with angle of sweep.

V. Discussion and Conclusions

All the experiments in this investigation were performed with attached flow on the wing surfaces at all times. Two mean freestream velocities of 12.43 and 20.00 m/s were used, resulting in low Reynolds numbers (up to 2×10^5 based on root chord) although transition strips on both surfaces simulated the boundary layer at higher Reynolds numbers. No wind tunnel corrections have been applied to the results presented here because of the difficulty of modeling the complex working section geometry of the gust tunnel (see Ref. 13). The steady lift, pitching moment, and rolling moment curve slopes are used as the zero frequency cases in the oscillatory flow tests.

The lift, pitching moment, and rolling moment amplitude variations ($\Delta C_L/\bar{w}_g$, $\Delta C_{PM}/\bar{w}_g$, and $\Delta C_{RM}/\bar{w}_g$) with frequency parameter ($\nu = \omega c/U$) for all the wings indicate that results for the two freestream velocities are closely consistent with each other in that they collapse onto the same curves when plotted in terms of frequency parameter. Furthermore, the oscillatory flow force amplitudes and phases were measured to be independent of wing incidence for attached flow. Data plotted in Fig. 10 indicate how the phase lags of lift (and consequently pitching moment) increase for higher wing sweep angles. This effect is to be expected since the gust distribution phase alters with distance downstream, thus influencing the swept wings which extend for a larger streamwise distance.

An overview of the force data at skew angles of 10 and 20 deg shows that the total lift and pitching moment amplitudes are not unduly affected, although the asymmetric lift distribution on the two wing halves generates significant rolling moments. As described earlier, the test wings were constructed with well-rounded streamwise tips. It was anticipated that an oblique gust may trigger a large contribution to rolling moment from the wing tips when they are no longer aligned at streamwise attitudes to the flow. However, the

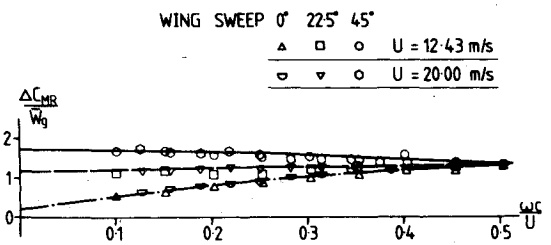

Fig. 11 Amplitude of oscillating rolling moment as a function of wing sweep for $\theta = 20$ deg.

rolling moment data indicate that the influence of the asymmetric sweep of the two wing halves and the streamwise phase lag of freestream gust incidence play dominant roles.

In the comparison of this experimental data with equivalent theoretical results, the traveling wave nature of the incident gust has to be accounted for. As indicated by Eq. (1), the experiments were conducted with a gust convection velocity of 0.61 of the freestream velocity. Most theoretical solutions are derived for an oscillatory gust convecting downstream with the freestream velocity. However, comparisons between theories based on gusts moving with the freestream velocity and the present experiments can be made by interpreting the change in gust encounter velocity as a change in "effective" frequency parameter ν', which for these experiments would have the value

$$\nu' = \omega c/0.61U = \nu/0.61 \tag{2}$$

References

[1] Ashley, H., "Unsteady Subsonic and Supersonic Inviscid Flow," AGARD Conference on Unsteady Aerodynamics, Ottawa, AGARD CP-227, Sept. 1977, pp. 1.1-1.32.

[2] McCroskey, W.J., "Some Current Research in Unsteady Fluid Dynamics," *Transactions of ASME, Journal of Fluids Engineering,* Ser. I, March 1977, pp. 8-39.

[3] Filotas, L.T., "Approximate Transfer Functions for Large Aspect Ratio Wings in Turbulent Flow," *Journal of Aircraft,* Vol. 8, June 1971, pp. 395-400.

[4] Hobbs, N.P., "The Transient Downwash Resulting from the Encounter of an Airfoil with a Moving Gust Field," *Journal of Aeronautical Sciences,* Vol. 24, Oct. 1957, pp. 731-740, 754.

[5] Patel, M.H., "Aerodynamic Forces on Finite Wings in Oscillatory Flow: An Experimental Study," *AIAA Journal,* Vol. 16, Nov. 1978, pp. 1175-1180.

[6] Patel, M.H., "The Delta Wing in Oscillatory Gusts," *AIAA Journal,* Vol. 18, May 1980, pp. 481-486.

[7] Patel, M.H., "On the Linear Superposition of Aerodynamic Forces on Wings in Periodic Gusts," *Aeronautical Journal,* Vol. 82, No. 810, June 1978, pp. 267-272.

[8] Commerford, G.I. and Carta, F.O., "Unsteady Aerodynamic Response of a Two-Dimensional Aerofoil at High Reduced Frequency," *AIAA Journal,* Vol. 12, Jan. 1974, pp. 43-48.

[9] Satyanarayana, B., Gostelow, J.P., and Henderson, P.E., "A Comparison Between Experimental and Theoretical Fluctuating Lift on Cascades at Low Frequency Parameters," ASME Paper 74-GT-78, March 1974.

[10] Fujita, H. and Kovasznay, L.S.G., "Unsteady Lift and Radiated Sound from a Wake Cutting Aerofoil," *AIAA Journal,* Vol. 12, Sept. 1974, pp. 1216-1221.

[11] Ho, C.M. and Kovasznay, L.S.G., "Wake Cutting by a Cascade of Cambered Blades," *Progress in Astronautics and Aeronautics,* Vol. 44, edited by I.R. Schwartz, MIT Press, Cambridge, Mass., 1976, pp. 43-53.

[12] Armandariz, M., Rachele, H., Jones, J. A., Essenwanger, D.M., "Effects of Surface Winds and Gusts on Aircraft Designe and Operation," AGARD R-626, Nov. 1974, pp. 1-88.

[13] Patel, M.H. and Hancock, G.J., "A Gust Tunnel Facility," Aeronautical Research Council, London, R&M 3802, 1977.

[14] Engineering Sciences Data Unit Sheet, "Lift Curve Slope and Aerodynamic Center Position of Wings in Inviscid Subsonic Flow," Item No. 70011, Engineering Sciences Data Unit, London.